Available online at www.sciencedirect.com
ScienceDirect
Journal of Nuclear Materials 373 (2008) 44–52
journal of nuclear materials
www.elsevier.com/locate/jnucmat

Influence of hydrogen on the corrosion behavior of stainless steels in lithium

A.V. Shulga

Moscow Engineering Physics Institute, State University, 31 Kashirskoe Sh., Moscow 115409, Russian Federation

Received 27 June 2006; accepted 17 April 2007

Abstract

Corrosion behavior of several stainless steels in lithium and lithium with 0.05%H has been examined. Corrosion tests were performed under static conditions at 600 and 700 °C in the austenitic stainless steel of the type AISI 304 containers. Intensive formation of σ-phase of the composition $Fe_{50}Cr_{43}Mo_3Ni_4$ on the surface of austenitic stainless steels of the type AISI 316 at 700 °C for 1000 h was established as a result of isothermal mass transfer. Addition of 0.05%H in the form of LiH to lithium resulted in an increase in the quantity of the σ-phase. After corrosion tests of ferritic/martensitic steel in lithium at 700 °C for 1000 h the formation of the γ-phase was observed. In Li + 0.05%H besides the γ-phase was also formed the σ-phase. The features of decarburization of investigated stainless steels were examined using the direct method of activation autoradiography on carbon. Addition of 0.05%H in lithium significantly decreased the carbon content in the decarburization zone of austenitic stainless steel Fe–18Cr–15Ni–0.15C–0.23B without a noticeable change in the thickness of the decarburization zone. Decarburization of ferritic/martensitic stainless steel was less than of austenitic stainless steel using the same corrosion tests.

1. Introduction

Molten lithium has been proposed as a suitable medium for tritium breeding in various designs of D-T fusion reactors and as an efficient coolant. Compatibility of structural materials, in particular of high strength and corrosion resistant stainless steels with liquid lithium, is one of the main requirement to achieve this purpose. The isothermal mass transfer processes of stainless steel components are an important factor in the corrosion behavior of stainless steels in liquid lithium [1–4]. The solubility of stainless steel components in liquid lithium plays an important role in mass transfer [1–4]. The goal of the present work was to examine the influence of hydrogen addition to lithium on the corrosion behavior of austenitic and ferritic/martensitic stainless steels at temperatures of 600 and 700 °C. Hydrogen doping was used to simulate a possible tritium effect.

2. Experimental procedures

The compositions of the investigated austenitic and ferritic/martensitic stainless steels are listed in Table 1. Two types of specimens in the form of coupons with different dimensions ($\sim 10 \times 10 \times 0.4$ mm and $\sim 10 \times 10 \times 3$) were used. The specimens of the first type in the form of thin coupons were produced from the cladding fuel tubes of type AISI 316 austenitic stainless steels (three variants of composition, Table 1) and ferritic/martensitic steel. Flat specimens of the first type were produced by straightening the rings cut from the cladding tubes. The outer surface of the cladding tubes in the state of their making was polished. Therefore, these specimens were tested without any additional preparation of their surfaces The specimens of the second type ($\sim 10 \times 10 \times 3$ mm) were cut from semi-finished

E-mail address: avshulga@mephi.ru

0022-3115/$ - see front matter © 2007 Elsevier B.V. All rights reserved.
doi:10.1016/j.jnucmat.2007.04.050

Table 1
Chemical composition of the investigated stainless steels

Material	Fe	Cr	Ni	Mo	Nb	Ti	V	C	B
EI 847 type AISI 316	Remaining	15.8	15.2	2.8	0.8			0.08	
EP 172 type AISI 316	–	15.9	15.1	2.8	0.8			0.08	0.008
16Cr–15Ni–3Mo–1Ti type AISI 316	–	16.1	15.3	2.9		0.8		0.08	
Fe–18Cr–15Ni–0.15C–0.23B	–	18.1	15.2					0.15	0.23
EP450	–	12.3	0.2	1.6	0.5		0.3	0.12	0.004
Fe–18Cr–10Ni–1Ti–0.12C type AISI 304	–	18.2	10.1			1.2		0.12	

All compositions are given in mass percent unless otherwise stated.

products (in the form of rods $\sim$ 50 mm in diameter) of the stainless steel EP 172 of the type AISI 316, ferritic/martensitic steel EP 450 and austenitic stainless steel Fe–18Cr–15Ni–0.15C–0.23B. The specimens of the second type were metallographically polished.

Corrosion tests of these materials were performed under static conditions. Concentration of hydrogen in lithium – 0.05%H was controlled in accordance with the phase diagram of the Li–H system by the addition of calculated quantities of chemically pure LiH. The stainless steel containers with lithium and Li + 0.05%H were used for corrosion test experiments. The chemical composition of the container material, a type AISI 304 austenitic stainless steel Fe–18Cr–10Ni–1Ti–0.12C, is also given in Table 1. The specimens were uniformly placed in a liquid environment within a container. They were suspended in a chain with the distance between neighbor specimens as $\geqslant$2 mm. The specimens of identical compositions were tested together in one container and the specimens of various compositions in different containers.

The corrosion tests were performed at the temperatures of 600 and 700 °C for 1400 and 1000 h, respectively. All loading operation was carried out in a glove box fabricated using Fe–18Cr–10Ni–1Ti–0.12C austenitic stainless steel in argon and was equipped with an arc welding device. After completion of the corrosion tests, lithium was removed from the specimens by washing with water and alcohol. For investigation of the structure and composition of the thin surface layer of the specimens, cross sections with a low angle (7°) from the surface were prepared by mechanical polishing. Low angle cross sections were used for a more detailed study of the thin surface layers of the specimens.

The specimens were studied by metallography, scanning electron microscopy (SEM), quantitative X-ray spectral microanalysis (XRSMA) via Camebax 226, qualitative X-ray phase analysis (QXRPA), and by an autoradiography method via cyclotron MEPhI.

In this work an autoradiography method on carbon has been used to obtain direct evidence for the distribution of carbon in decarburization/carburization zones in the form of solid solution and carbide particles. This nuclear method has a high sensitivity and allows investigation of the carbon distribution with a high spatial resolution. The autoradiography method on carbon is based on the use of the nuclear reaction $^{12}C(d,n)\,^{13}N$ on carbon atoms with 2 MeV deuterons. Secondary β-particles were detected by a nuclear photographic emulsion on the specimen surface.

3. Results and discussion

The investigation of the microstructure of the austenitic stainless steels of the type AISI 316 (three variants of composition, Table 1) after corrosion tests in lithium and lithium with hydrogen (Li + 0.05%H) at 700 °C for 1000 h has shown the formation of new crystals on the surface of the specimens. Figs. 1 and 2 show the surface layer microstructure of the type AISI 316 austenitic stainless steel EP 172 as the microstructure with typical kinds of these crystals for all three variants of the steels with small variants of composition.

The QXRPA methods allowed one to determine these crystals on the surface of the samples tested in lithium and in lithium with 0.05% hydrogen as the σ-phase (Fig. 3(a–c)). Experimentally determined lattice parameters of the σ-phase $a = 0.884$ nm, $c = 0.455$ nm that are in agreement with the data presented in work [5] for compound $Fe_{53.5}Cr_{46.5}$. The XRSMA permitted one to determine the composition of σ-phase crystals as ($Fe_{50}Cr_{43}Mo_3Ni_4$) that corresponds the concentrations of iron – 50, chrome – 40, molybdenum – 5 and nickel – 4 wt%. This averaged composition of σ-phase crystals was established via quantitative analysis, in different points, of a number of σ-phase crystals. The presence of molybdenum and nickel in the σ-phase results in some increase of the lattice parameter (a) in comparison with the lattice parameter for $Fe_{53.5}Cr_{46.5}$ [5] ($a = 0.8799$ nm, $c = 0.4544$ nm).

It was found that dimensions and density of the spatial distribution of the σ-phase crystals formed under corrosion test in Li were significantly different from those formed in Li + 0.05%H.

After corrosion tests in lithium, large ($\sim$100 μm) and widely spaced crystals of the σ-phase with a clear crystalline form were observed (Figs. 1(a), (b), (d), and 2(a)). The arrows on the enumerated figures show large and separate crystals of σ-phase. The metallographic investigation of the specimens with low angle cross sections permits us to investigate the topography of the surface area close to the cross section that allows the determination of the dependence between surface topography features (such as σ-

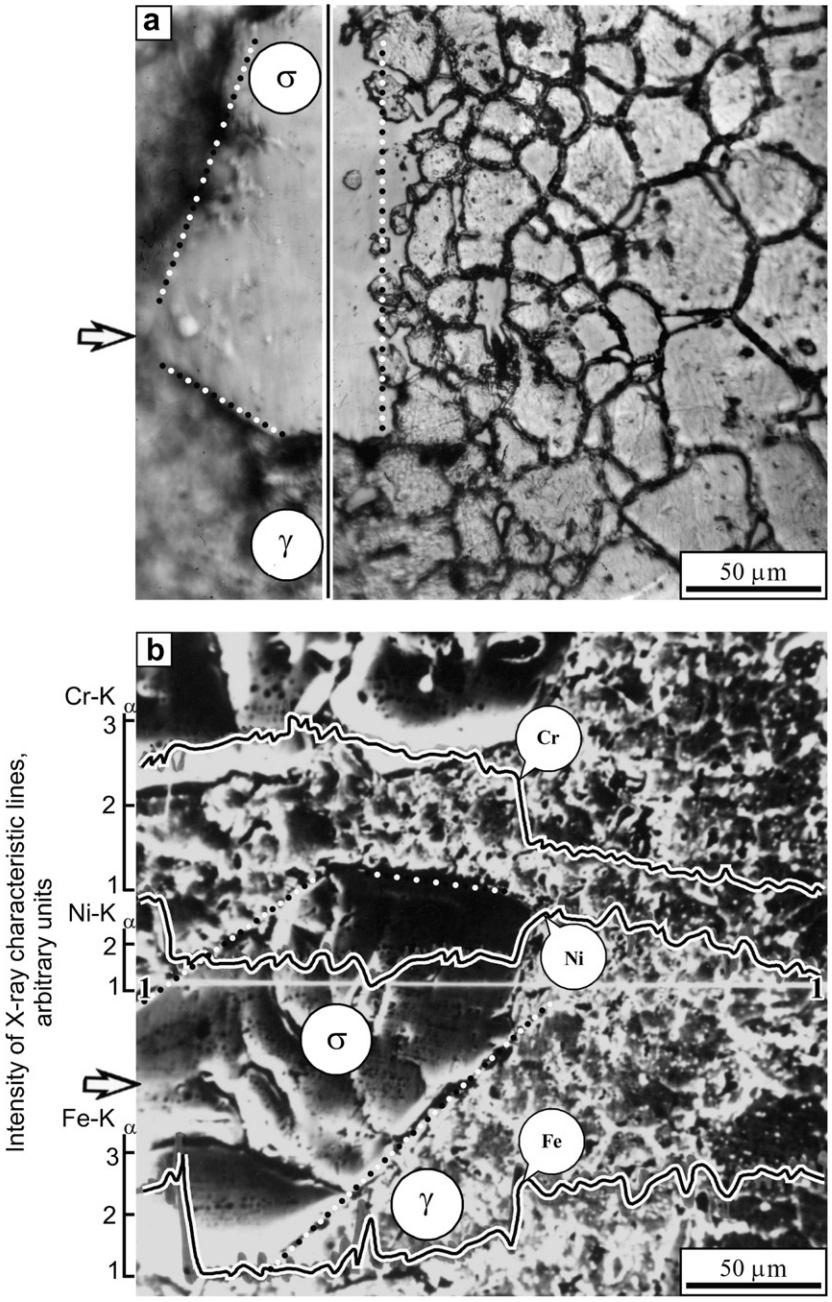

Fig. 1. Microstructure of the surface layer of austenitic stainless steel EP 172 of the type AISI 316 after corrosion tests in austenitic stainless steel (Fe–18Cr–10Ni–1Ti–0.12C) of the type AISI 304 container with lithium (a, b, d) and Li + 0.05%H (c, e) at 700 °C for 1000 h: (a, c, d, e) metallographic micrographs of the surface (on the left) and a low angle (7°) cross section of the specimen (on the right); (b) scanning electron microscopy micrograph of the same specimen with curves of intensity of characteristic X-ray lines K_α from chromium, nickel and iron obtained by XRSMA along the line 1–1. Dotted lines surround the σ-phase crystals.

phase crystals) and those of the microstructure cross sections.

Fig. 1(b) illustrates the variations of intensity of X-ray characteristic lines from Cr, Ni, and Fe along the line 1–1 intersecting the σ-phase crystal. These variations correspond an increase in the Cr content and a decrease in the Ni and Fe contents in the volume of the σ-phase crystal in comparison with that of the austenitic γ-matrix. These variations correlate with the averaged σ-phase composition and the γ-matrix composition of the type AISI 316 investigated stainless steel.

After the corrosion test in Li + 0.05%H, the noticeably more dispersed crystals (~20 μm) of the σ-phase with a high density of distribution, which formed a continuous layer on the surface of specimens, were established (Figs. 1(c) and (e) and 2(b)). The small arrows on these figures show the dispersed crystals of σ-phase with a high density of distribution.

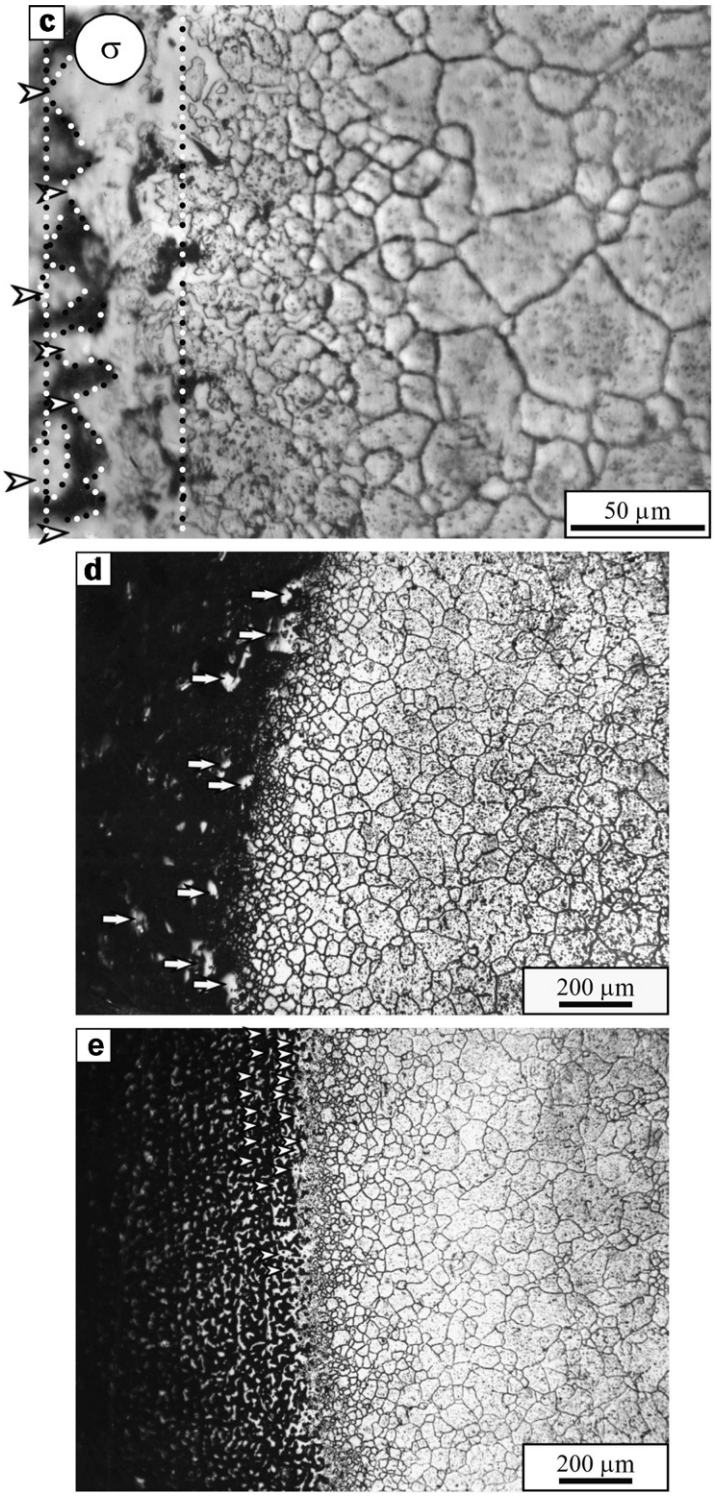

Fig. 1 (*continued*)

The peculiarities of σ-phase formation in Li and Li + 0.05%H do not noticeably depend on the small variants of the composition of the type AISI 316 investigated steels and the structural states of specimens (cut from both the cladding tubes and the rods).

Figs. 1 and 2 specifically show the surface microstructure of austenitic stainless steel EP 172 specimens cut from the cladding tube.

The QXRPA shows (Fig. 3) that a higher amount of the σ-phase was formed in Li + 0.05%H than that in lithium.

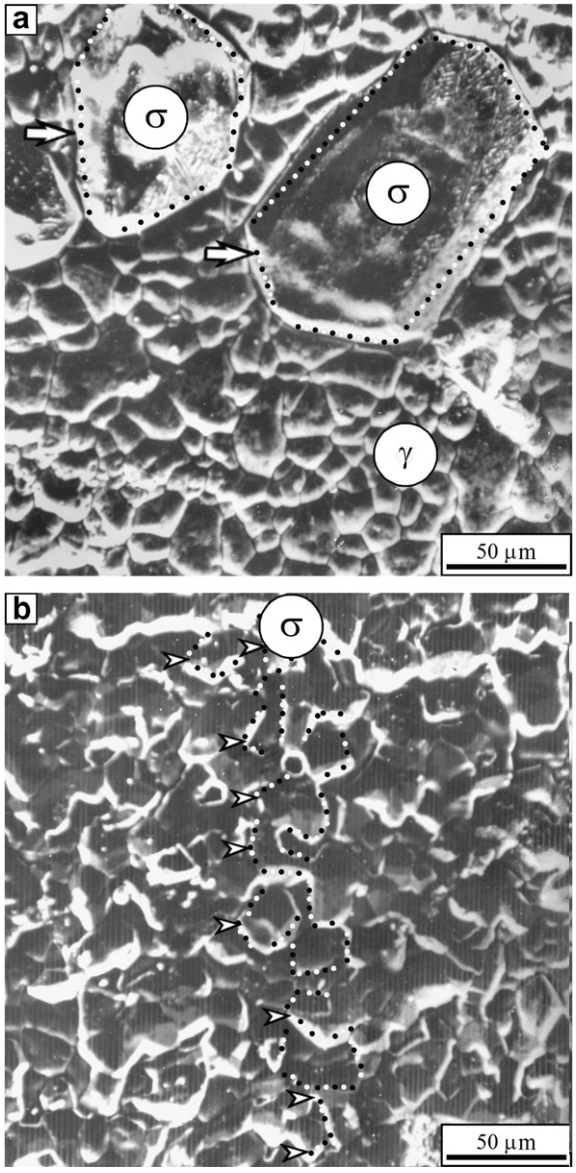

Fig. 2. Topography of the surface of austenitic stainless steel EP 172 of the type AISI 316 after corrosion tests in lithium (a) and in Li + 0.05%H (b) at 700 °C for 1000 h (SEM micrographs). Dotted lines surround the σ-phase crystals.

The presence of the γ-phase diffraction lines with higher intensities after the corrosion tests in lithium than in Li + 0.05%H is in agreement with the assumption that a continuous layer of the σ-phase on the surface of specimens after corrosion in Li + 0.05%H noticeably decreases the intensities of the γ-phase diffraction lines, since it is under the σ-phase continuous layer.

The formation of the σ-phase on austenitic stainless steels of the type AISI 316 under corrosion tests at 700 °C for 1000 h using containers of the type AISI 304 with Li and Li + 0.05%H has confirmed the estimated mass transfer directions of the stainless steel components. The mass transfer of chromium should be directed from the container to the specimen and in the case of nickel, molybdenum – in the reverse direction. The anticipated directions of isothermal mass transfer under corrosion tests can be estimated from the chemical potential of alloying elements in specimens and in the container material. In the first approximation its value is proportional to the content of elements in the specimens and in the container material.

The σ-phase crystals on the specimen surface grow in the outer direction as well as in the inner direction as shown in Fig. 1(a). The vertical line designates the boundary line between the initial surface of the specimen and the inner layers of the cross section. The σ-phase crystal growth in the outer direction from the initial surface presumably was resulted from the mass transfer of chromium from the container and deposition on the specimen surface. The σ-phase growth in the inner direction from the surface of the specimens may be associated with dissolution of nickel in lithium and diffusion of molybdenum from the bulk of the specimen to the surface.

The microstructure of the surface layer of the specimen after the corrosion test in lithium is characterized by the formation of relatively large subgrains separated with thick boundaries, presumably as a result of initial grain disintegration and growth of σ-phase crystals in the inner direction. The formation of noticeably smaller subgrains separated with thinner boundaries in Li + 0.05%H than in lithium (Fig. 1) is a result of more homogeneous nucleation of the σ-phase crystals. This result is consistent with the noticeable effect of hydrogen on the grain boundary attack of austenitic stainless steels in AISI 304 stainless steel containers reported in the work [3]. Thus, hydrogen has a noticeable effect on the competition between solubility-driven mass transport and the surface chemical reactions [2]. Hydrogen stimulates the chemical reactions homogeneously on the surface with participation of chromium, and therefore suppresses the inhomogeneous grain boundary attack of austenitic stainless steels.

The formation of the σ-phase besides the γ-phase under corrosion tests of ferritic/martensitic stainless steel in Li + 0.05%H at 700 °C for 1000 h (Fig. 3(d)) was established. In lithium on the surface of the specimen of ferritic/martensitic stainless steel almost entirely the γ-phase was formed (Fig. 3(e)). The appearance of some amount of the γ-phase was observed in lithium at 600 °C for 1400 h (Fig. 3(f)).

Intensive formation of the σ-phase on the surface of ferritic/martensitic stainless steel in Li + 0.05%H under the corrosion test at 700 °C for 1000 h and formation of almost entirely the γ-phase in lithium, possibly resulted from an intensive mass transfer of chromium in Li + 0.05%H and predominately of nickel in lithium. Since the effect of hydrogen on the solubility of chromium in Li at 700 °C is not essential [4], consequently, the solubility-driven mass transfer of nickel dominates in lithium, whereas in Li + 0.05%H intensive mass transfer also occurred, controlled by the chemical reaction with chromium participation.

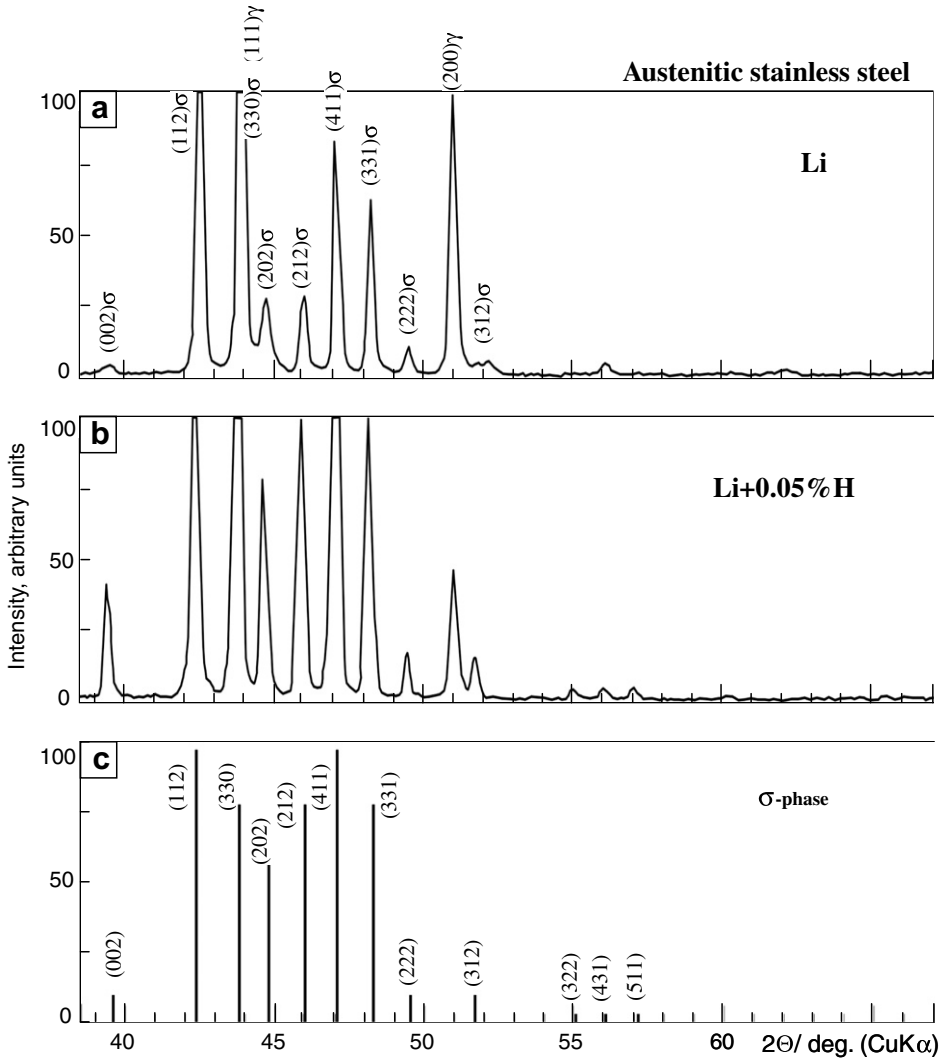

Fig. 3. XRD patterns of the specimens of austenitic stainless steel EP 172 of the type AISI 316 after corrosion tests in lithium (a) and in Li + 0.05%H; (b) at 700 °C for 1000 h; (c) scheme of XRD patterns of the σ-phase with composition $Fe_{53.5}Cr_{46.5}$ [5]; (d, e, f) XRD patterns of ferritic/martensitic stainless steel EP 450 after the corrosion tests.

Thus, hydrogen stimulates the increase of the isothermal mass transfer of chromium on austenitic steel of the type AISI 316 and ferritic/martensitic stainless steels with the formation of the σ-phase.

Under corrosion test in lithium at 700 °C for 1000 h austenitic stainless steel Fe–18Cr–15Ni–0.15C–0.23B was significantly decarburized. The autoradiograph on carbon (Fig. 4(a)) shows a decarburized layer (thickness $d/10 \sim 70$ μm) with a lower concentration of carbon, than in the bulk of the specimen. In Li + 0.05%H this layer was characterized by the same thickness ($d/10 \sim 70$ μm) and the low concentration of carbon in solid solution without carbide particles (Fig. 4(b)), whereas after tests in liquid lithium in the decarburization zone the several carbide particles and a higher concentration of carbon in the form of solid solution were observed. Thus, the hydrogen addition to lithium leads to an increase in the intensity of the carbon depletion without a noticeable increasing of the thickness of the decarburized layer.

Decarburization of ferritic/martensitic stainless steel EP450 occurs to a lower degree with the formation of a thinner layer (thickness ~20 μm) than in the case of austenitic stainless steel Fe–18Cr–15Ni–0.15C–0.23B in the same corrosion tests in Li + 0.05%H at 700 °C for 1000 h (Fig. 4(c)). These specimens of both steels were cut from rods. This result suggests that decarburization of stainless steels under corrosion tests in lithium is not a diffusion controlled process, as the diffusivity of carbon and substitutional carbide forming components in the ferritic body centered lattice is higher than in the austenitic close packed face centered lattice. Consequently, the carbide stability, presumably, has a principal effect on the decarburization of steels.

According to Ref. [2], the intensity of carbon transport in the ferritic steel/lithium system depends on alloying of

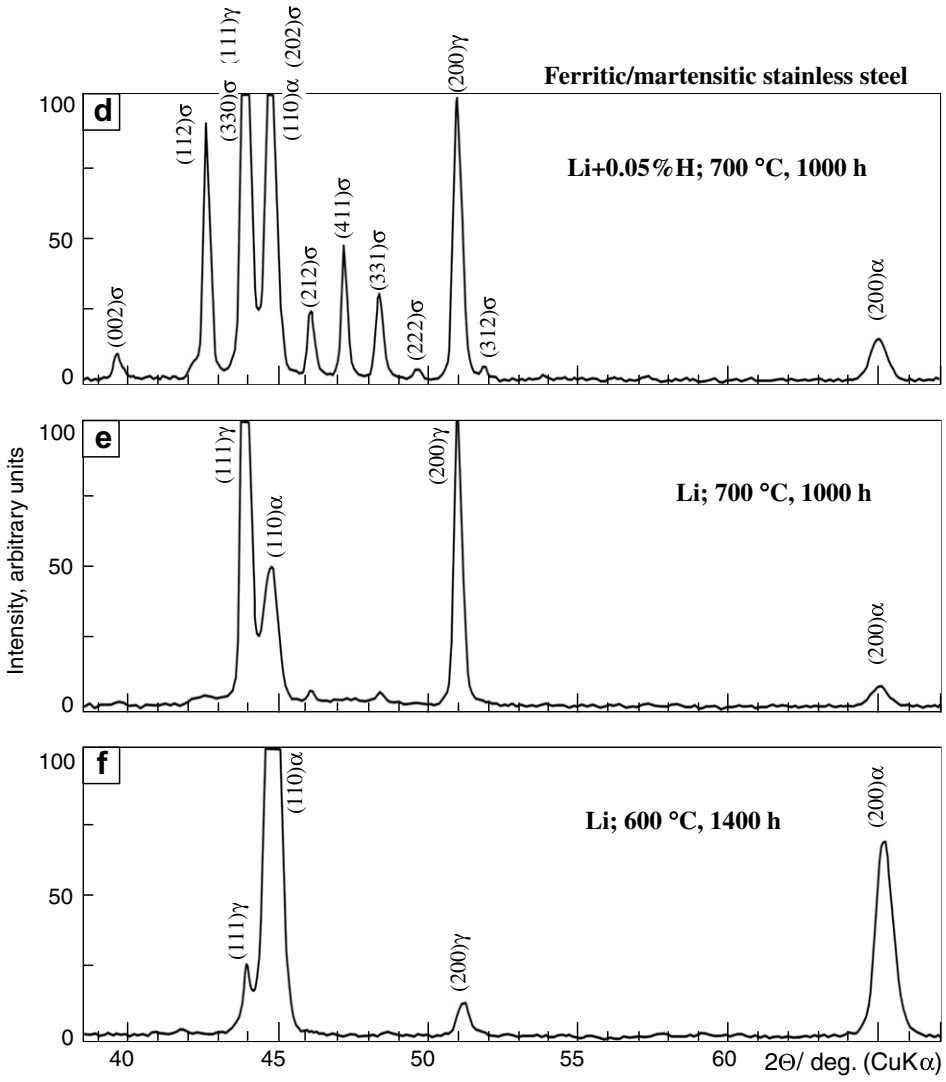

Fig. 3 (*continued*)

the ferritic steels by strong carbide forming elements (vanadium and titanium) with the formation of more stable carbides than $(Fe, Cr)_{23}C_6$. Consequently, a more stable carbide of the type MC and presumably $M_{23}C_6$ with a high content of chromium in ferritic/martensitic stainless steel EP 450 than in austenitic stainless steel Fe–18Cr–15Ni–0.15C–0.23B results in the lower decarburization of ferritic/martensitic stainless steel.

An important particularity of the autoradiographs of decarburized specimens is the presence of a thin layer, the nearest to the surface, with a higher concentration of carbon in the form of a layer of carbide particles besides the deep zone of carbon depletion (Fig. 4). Formation of this thin layer with a higher content of carbon can be explained by the mechanism of decarburization in the lithium environment via chemical reaction on carbide particles that results in the formation of an intermediate product, which is dissolved later on.

Because of the high affinity of carbon for hydrogen [6], the hydrogen can also directly interact with carbon and form hydrocarbons (e.g., CH_4), which stimulates decarburization. The effect of hydrogen may be also connected with some increase in the solubility of carbon in lithium according to Ref. [4].

4. Conclusion

In this work the corrosion tests of austenitic and ferritic/martensitic stainless steels in liquid lithium and Li + 0.05%H were carried out. Modifications were found for the structure and composition of the surface layers of stainless steels as a result of isothermal mass transfer between the stainless steel specimens and the type AISI 304 container material, as follows:

1. On the surface of the austenitic stainless steels of the type AISI 316 in lithium was formed the σ-phase ($Fe_{50}Cr_{43}Mo_3Ni_4$) at 700 °C for 1000 h. The σ-phase crystal growth in the outer direction from the surface of the specimens presumably resulted from the deposition

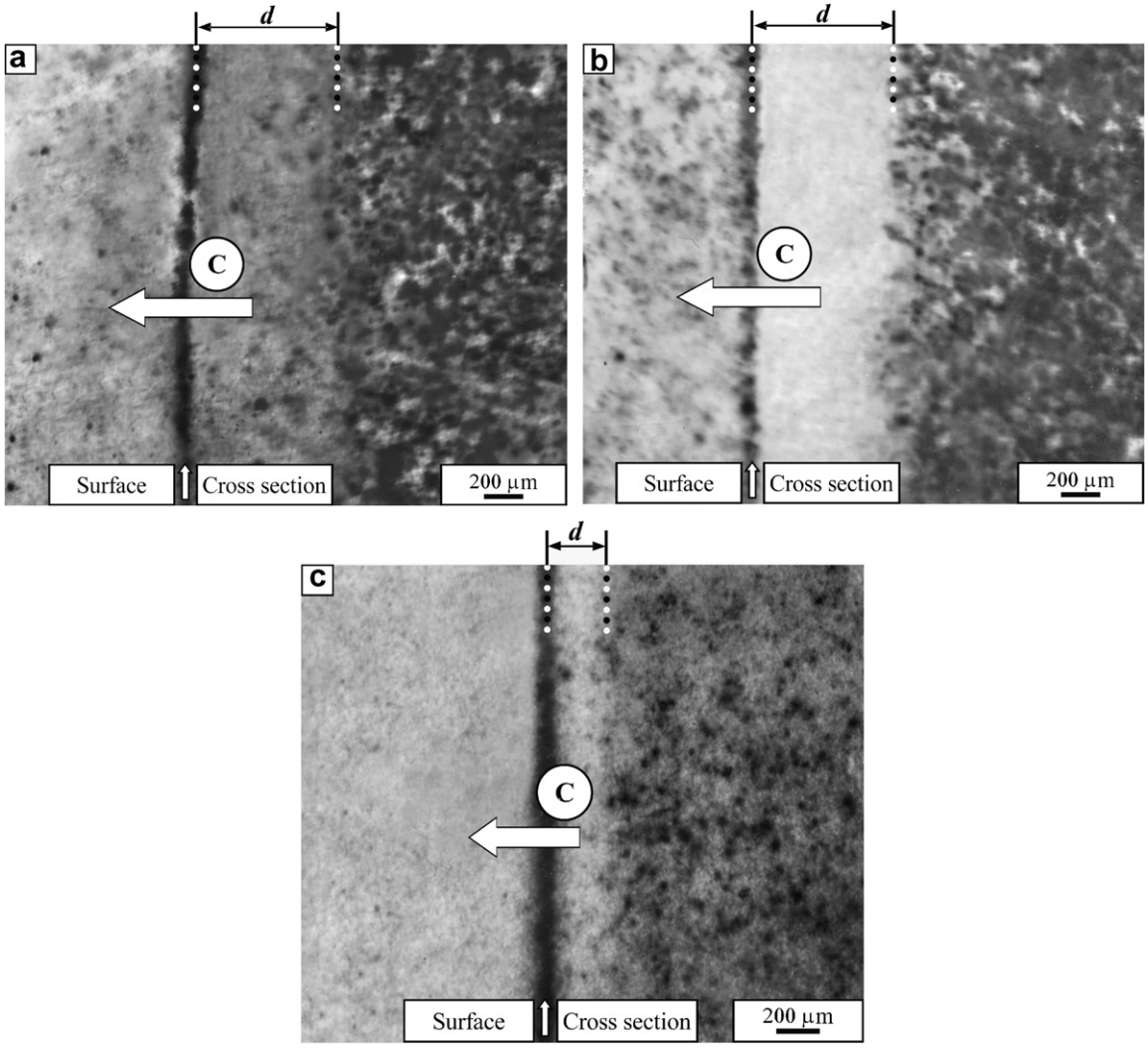

Fig. 4. Activation autoradiographs of carbon distribution in surface layers at the low angle cross section of the specimen of austenitic stainless steel Fe–18Cr–15Ni–0.15C–0.23B; (a, b) and ferritic/martensitic stainless steel EP 450; (c) after corrosion tests in lithium; (a) and in Li + 0.05%H; (b, c) at 700 °C for 1000 h. In this work the photographs of the autoradiograph are positive; therefore dark/bright areas correspond to more/less concentration of carbon. Vertical arrows show the boundary between the surface of the specimens and the cross section. Large horizontal arrows show directions of the mass transfer of carbon from investigated steels. d is the length of the decarburization zones on the planes of the low angle cross sections; therefore $d \cdot \sin 7^\circ \sim d/10$ is the thickness of the decarburization zones.

of chromium and in the inner direction owing to diffusion to the surface of molybdenum and depletion of nickel in lithium.

2. Addition of 0.05% hydrogen to lithium had an appreciable effect on the formation of the σ-phase and on the grain boundary attack. The σ-phase crystals formed under corrosion tests in lithium are large with a low surface density and usually have a clear crystalline form. The σ-phase crystals under corrosion tests in Li + 0.05%H were finer, more homogeneous and characterized by a high density of distribution with formation of a continuous layer. A higher amount of the σ-phase was formed under corrosion tests in Li + 0.05%H than in lithium. The hydrogen addition in lithium stimulated the isothermal mass transfer of chromium with the formation of the σ-phase on austenitic and ferritic/martensitic stainless steels.
3. Depletion of carbon from the specimens of the stainless steels Fe–18Cr–15Ni–0.15C–0.23B and EP450 at 700 °C for 1000 h in Li + 0.05%H was more intensive than in the lithium environment. The carbon content in the decarburization zone under corrosion tests in Li + 0.05%H noticeably decreased in comparison with lithium, but no essential distinctions of decarburization zone thickness were observed.
4. A significantly lower decarburization of ferritic/martensitic stainless steel EP450 than austenitic stainless steel Fe–18Cr–15Ni–0.15C–0.23B under the same corrosion tests suggests that the carbon depletion from these stainless steels as well as from carbon steels is not a diffusion controlled process, but depends on the carbide

stability. The more stable carbide in ferritic/martensitic stainless steel than in austenitic stainless steel provides, in accordance with Ref. [2], the lower decarburization of ferritic/martensitic steel in comparison with austenitic stainless steel.

5. A thin surface layer enriched with carbon in the form of a monolayer of dispersed carbide particles was detected on the surface of decarburized stainless steels. This result suggests that the chemical reactions on carbide particles with the formation of intermediate (soluble) products, presumably, are the determining stage for decarburization.

References

[1] P.F. Tortorelli, J. Nucl. Mater. 191–194 (1992) 965.
[2] T. Flament, P. Tortorelli, V. Coen, H.U. Borgstedt, J. Nucl. Mater. 191–194 (1992) 132.
[3] V. Coen, H. Kolbe, L. Orecchia, T. Sasaki, J. Nucl. Mater. 85&86 (1979) 271.
[4] V.N. Michailov, V.A. Evtikhin, I.E. Lublinski, A.V. Vertkov, A.N. Chumanov, Lithium for Fusion Reactors and Space Nuclear Power Systems of XXI Century, Energoatomizdat, Moscow, 1999, p. 81.
[5] E.O. Hall, S.H. Algie, J. Inst. Met. 94 (April) (1966) 61.
[6] O. Kubaschewski, C.B. Alcock, Metallurgical thermochemistry, Pergamon Press Ltd., Oxford, England, 1979.